Catalysis Today 175 (2011) 610–614

Contents lists available at ScienceDirect

Catalysis Today

journal homepage: www.elsevier.com/locate/cattod

The effects of Bi_2O_3 on the CO oxidation over Co_3O_4

Yang Lou, Li Wang*, Yanhui Zhang, Zhenyang Zhao, Zhigang Zhang, Guanzhong Lu, Yun Guo*

Laboratory for Advanced Materials, Research Institute of Industrial Catalysis, East China University of Science and Technology, Shanghai 200237, China

ARTICLE INFO

Article history:
Received 31 October 2010
Received in revised form 21 February 2011
Accepted 30 March 2011
Available online 4 May 2011

Keywords:
Co_3O_4
Bi_2O_3
CO oxidation
Oxygen vacancy

ABSTRACT

The Co_3O_4 and Bi_2O_3–Co_3O_4 were prepared by precipitation and co-precipitation method. The samples were characterized by XRD, BET, H_2-TPR, Raman, XPS and EPR. The low-temperature CO oxidation on the catalysts was also investigated. The results showed the deposition of Bi_2O_3 enhanced the activity and stability of Co_3O_4 for CO oxidation. 20 wt.% Bi_2O_3–Co_3O_4 could completely convert CO as low as −89 °C, and maintain the complete oxidation of CO at −75 °C for 10 h. XRD and Raman results showed Bi_2O_3 could enter the lattice of Co_3O_4, and promote the formation of the lattice distortion and structural defect. H_2-TPR results showed that reduction of Co_3O_4 was promoted and the diffusion of oxygen was accelerated. XPS and EPR results showed the surface richness of Co^{3+} and the increase of Co^{2+} in 20 wt.% Bi_2O_3–Co_3O_4. The formation of more Co^{2+} in 20 wt.% Bi_2O_3–Co_3O_4 could produce structure defects and lead to the formation of more oxygen vacancy, which was suggested to play the critical role in promoting the catalytic activity and stability of 20 wt.% Bi_2O_3–Co_3O_4.

1. Introduction

CO catalytic oxidation has drawn great attention due to its wide application and academic studies in the catalysis field [1–4]. Supported noble metal catalysts show very high activity for CO oxidation. Among them, the gold catalysts behaved extraordinarily active for low temperature CO oxidation [3]. Goodman and coworker [4] investigated the effect of catalyst structure on the CO oxidation activity over Au/TiO_2. Qiao et al. [5] prepared a ferric hydroxide supported Pd catalyst over which total oxidation of CO could be achieved at −15 °C. Li et al. [2] reported that Pt/Fe_2O_3 can completely transform CO into CO_2 at room temperature in the presence of water vapor for more than 3000 h. But the high cost of noble metals limited the application of supported noble metal catalysts.

Co_3O_4 was considered as an alternative to noble metal and behaved very high activity for low-temperature CO oxidation under dry feed gas condition [6–10]. Co_3O_4 is one kind of transition metal oxides with spinel-type structure, containing Co^{3+} in an octahedral coordination and Co^{2+} in a tetrahedral coordination [10]. For CO oxidation over Co_3O_4, only Co^{3+} was supposed to have the activity [10–12]. The DFT study also proposed that CO was adsorbed on the surface-exposed Co^{3+} site [13]. Shen et al. [10] prepared Co_3O_4 nanorods with predominantly exposing (110) planes through the morphology control, which could completely oxidize CO as low as −77 °C due to the richness of active Co^{3+} sites on the surface. In general, the enhancement of CO adsorption and activation is beneficial for CO oxidation over Co_3O_4.

The activation of O_2 is also another key factor for CO oxidation by O_2. For example, the adsorption and activation of O_2 on supported Au catalysts was regard as a rate-limiting step since oxygen dissociation was inhibited on single gold crystals [5]. The high activity of the support to supply reactive oxygen was also suggested as the origin of $Au/Mg(OH)_2$ and Au/MgO catalysts, which exhibited high activity for low temperature CO oxidation even at −89 °C [14]. Liu et al. [15] proposed that a large amount of oxygen adsorbed on the FeO_x support was accounted for the high activity of supported Pt and Pd catalysts for low-temperature CO oxidation. The surface oxygen state has also great effects on the activity and deactivation of Co_3O_4, and the pretreatment conditions can influence its surface state. The CO oxidation activity increased and the deactivation rate suppressed with the increase of O_2 concentration [9,16]. The activity of preoxidized Co_3O_4 was much higher than the prereduced one [17]. Yu et al. [18] reported that the activity for CO oxidation over Co_3O_4 could be enhanced by promoting the activation of O_2 after pretreatment at moderate temperature.

Hence if the adsorption, dissociation and activation of O_2 could be enhanced, the activity and stability of CO oxidation over Co_3O_4 were suggested to be improved. Oxygen vacancy played a very important role in activating oxygen [19–21]. Shapovalov and Metiu [20] proposed that the oxygen vacancy could adsorb oxygen from the gas and weaken its bond. At the same time, the diffusion of activated oxygen could be accelerated due to the good mobility of surface vacancy [22].

In this paper, Co_3O_4 and 20 wt.% Bi_2O_3–Co_3O_4 were prepared and the activities for CO oxidation were investigated. The X-ray

* Corresponding author. Tel.: +86 21 64253703.
E-mail addresses: wangli@ecust.edu.cn (L. Wang), yunguo@ecust.edu.cn (Y. Guo).

0920-5861/$ – see front matter © 2011 Elsevier B.V. All rights reserved.
doi:10.1016/j.cattod.2011.03.064

diffraction (XRD), BET surface, Raman, X-ray photoelectron spectroscopy (XPS), Electron Paramagnetic Resonance (EPR) and H_2 temperature programmed reduction (H_2-TPR) were used to study the effects of Bi_2O_3 on the structure, surface properties and redox properties.

2. Experimental

2.1. Catalyst preparation

The Co_3O_4 and Bi_2O_3–Co_3O_4 were prepared by precipitation and co-precipitation method, respectively. The cobalt acetate ($Co(CH_3COO)_2{\cdot}4H_2O$) and bismuth chloride ($BiCl_3$) were used as precursor salts, and sodium carbonate(Na_2CO_3) was used as precipitant. The preparation method was similar to Ref. [10]. 4.98 g cobalt acetate and matching bismuth chloride were dissolved into 80 ml ethylene glycol, and the system was degassed by vacuum. Then the mixture was heated to 160 °C and kept in N_2 flow for 40 min. 200 ml of 0.22 M Na_2CO_3 solution heated at 80 °C was added into the above solution prepared, and mixture was further aged at 160 °C for 1 h under vigorously stirring. The precipitate was washed using distilled water until no Cl^- was detected by $AgNO_3$. After filtering, the solid powder obtained was dried at 65 °C overnight and calcined at 350 °C for 4 h in air. The calculated contents of Bi_2O_3 were 15, 20 and 25 wt.%.

2.2. Catalyst characterization

The XRD patterns of catalysts were obtained with Rigaku D/max 2550 VB/PC diffractometer using a Cu Kα radiation (λ = 1.54056 Å). The X-ray tube was operated at 40 kV and 40 mA. The intensity data were collected in a 2θ range from 10° to 80° with a scan rate of 6°/min.

The surface area was measured by nitrogen adsorption at liquid nitrogen temperature using a Quantachrome NOVA 4000e apparatus. Before measurement, the samples were degassed at 180 °C for 6 h in vacuum.

The X-ray photoelectron spectroscopy (XPS) analysis of 20 wt.% Bi_2O_3–Co_3O_4 and pure Co_3O_4 catalysts were performed with a Thermo ESCALAB 250. The spectra were excited by the Al Kα source (1486.6 eV). The binding energy was calibrated with respect to the C 1s peak energy set at 284.8 eV arising from adventitious carbon.

The temperature-programmed reduction (TPR) experiments were performed with a commercial temperature-programming system. 50 mg of the catalyst was heated in the flow of 5 vol.% H_2/N_2 (20 ml/min) at a heating rate of 10 °C/min from room temperature to 850 °C. The amount of H_2 uptake during the reduction was measured by thermal conductivity detector (TCD). Before experiments, the samples were pretreated at 350 °C for 40 min in 20 vol.% O_2/N_2.

Raman spectra were recorded with thin wafer on a Renishaw spectrometer using a 514 nm Ar^+ laser as the excitation source at room temperature. The laser beam intensity and the spectrum slit width were 2 mW and 3.5 cm^{-1}, respectively.

The EPR spectra were obtained by a Bruker EMX-8/2.7 EPR Spectrometer. Before the experiments, the samples were pretreated at 350 °C for 40 min using 20 vol.% O_2/N_2 (50 ml/min).

2.3. Evaluation of the catalytic performance

The activity of catalyst for CO oxidation was evaluated in a fixed-bed reactor at atmosphere pressure, and 200 mg catalyst (40–60 mesh) was used. The feed gas of 1 vol.% CO and 20 vol.% O_2 in N_2 passed though the catalytic bed at a flow rate of 50 ml/min. Before the experiments, the catalyst was pretreated at 350 °C for 40 min in 20 vol.% O_2/N_2 (50 ml/min). The dry feed gas was obtained by passing the feed gas though molecular-sieve trap cooled to −80 °C. The conversion of CO was measured from room temperature to the temperature of CO conversion below 20%. The temperature was controlled by using ethanol and liquid nitrogen mixture. The concentrations of CO and CO_2 in the outlet stream were measured by an on-line gas chromatograph after the catalyst bed temperature stabilized at the settled value for 15 min to obtain the steady state.

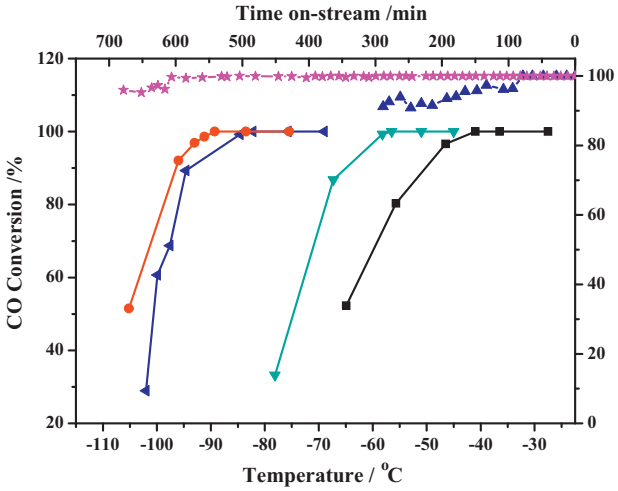

Fig. 1. The effect of doped content of Bi_2O_3 on the catalytic activity, (■) pure Co_3O_4; (◄) 15 wt.% Bi_2O_3–Co_3O_4; (●) 20 wt.% Bi_2O_3–Co_3O_4; (▼) 25 wt.% Bi_2O_3–Co_3O_4; (▲) the stability of pure Co_3O_4 was measured at −40 °C under dry condition; (★) the stability of 20 wt.% Bi_2O_3–Co_3O_4 was measured at −75 °C under dry condition.

3. Results and discussion

3.1. The catalytic activities of Co_3O_4 and Bi_2O_3–Co_3O_4

The catalytic performances of CO oxidation over pure Co_3O_4 and Bi_2O_3–Co_3O_4 are showed in Fig. 1. Pure Co_3O_4 showed good activity for CO oxidation, and the lowest temperature of complete conversion (LTCC) of CO was −40 °C. The catalytic activity of Bi_2O_3–Co_3O_4 was improved with the increase of Bi_2O_3 content up to 20%. 20 wt.% Bi_2O_3–Co_3O_4 catalyst behaved the highest activity and the LTCC of CO was as low as −89 °C. Continuously increasing the Bi_2O_3 content, the activity of catalyst decreased significantly. At the same time, the stability of Co_3O_4 was enhanced by the doped Bi_2O_3 greatly. Under dry feed gas condition, the complete CO conversion was maintained at −40 °C for 80 min over pure Co_3O_4, while 20 wt.% Bi_2O_3–Co_3O_4 could completely oxidize CO at −75 °C for 600 min.

3.2. Structure properties

XRD patterns of the 20 wt.% Bi_2O_3–Co_3O_4 and pure Co_3O_4 are shown in Fig. 2. For 20 wt.% Bi_2O_3–Co_3O_4, the characteristic peaks of Bi_2O_3 were observed at about 30.46 and 32.79°, and the diffraction peaks of Co_3O_4 behaved a slight shift. It indicated that the Bi^{3+} inserted the lattice of Co_3O_4 in the preparation process, and changed the lattice parameter of Co_3O_4 due to the larger radius of Bi^{3+} (r = 0.103 nm). At the same time, the characteristic peak of Co_3O_4 became broad obviously after the deposition of Bi_2O_3, which revealed the reduction of particle size. The crystalline sizes of pure Co_3O_4 and 20 wt.% Bi_2O_3–Co_3O_4 calculated based on Scherrer equation were 7.3 and 5.4 nm, respectively. It was implied that the insertion of Bi_2O_3 induced the structure defect of Co_3O_4 and suppressed the growth of crystal.

The BET surface area of Co_3O_4 prepared was 121.6 m^2/g. The deposition of Bi_2O_3 increased the surface area of Co_3O_4 significantly. The surface area of 20 wt.% Bi_2O_3–Co_3O_4 was 133.6 m^2/g.

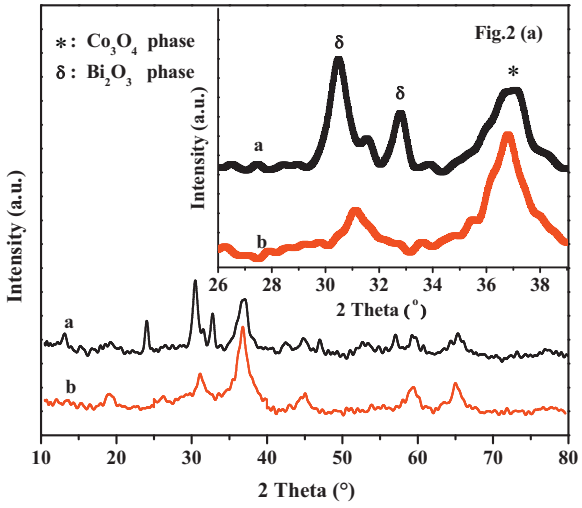

Fig. 2. XRD patterns of 20 wt.% Bi_2O_3–Co_3O_4 (a) and pure Co_3O_4 (b).

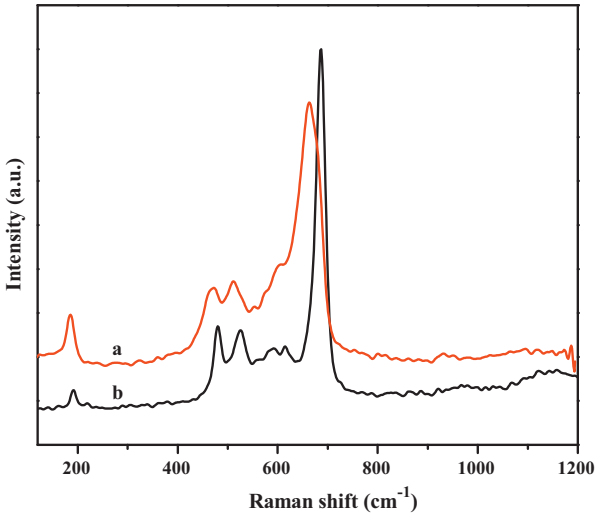

Fig. 4. Raman spectra of 20 wt.% Bi_2O_3–Co_3O_4 (a) and pure Co_3O_4 (b).

Combined with the results of XRD, the increase of surface area was suggested to be related to the small particle size of 20 wt.% Bi_2O_3–Co_3O_4. In general, the larger surface area and smaller grain size can supply more sites for CO and O_2 adsorption, which could promote CO and O_2 activation.

3.3. H_2-TPR

The TPR profiles of Co_3O_4, Bi_2O_3 and 20 wt.% Bi_2O_3–Co_3O_4 are shown in Fig. 3. There was a broad reduction peak at the temperature range at 350–600 °C over Bi_2O_3. Three peaks were observed on Co_3O_4. Among them, the peak at 130 °C (α_1) should be attributed to the reduction of surface oxygen species, the peak at 320 °C (α_2) was attributed to the reduction of Co^{3+} to Co^{2+}, and the peak at 625 °C (α_3) was aroused by the reduction of Co^{2+} [23–27]. Yu et al. [18] reported that there were four kinds of oxygen species in O_2-TPD, molecular oxygen species adsorbed on oxygen vacancy, surface oxygen ion bound with Co^{2+} and Co^{3+}, surface oxygen ion bound with three Co^{3+} cations and bulk oxygen, respectively. Hence, the peaks α_1, α_2, α_3 in H_2-TPR were suggested to be assigned to the reaction of H_2 with oxygen species adsorbed on surface, oxygen species bound with Co^{3+} cation and bulk oxygen, respectively.

For the reduction of 20 wt.% Bi_2O_3–Co_3O_4, the reduction peak β_2 corresponded to the reduction of Co^{3+} shifted slightly to the lower temperature. The new peak β_3 at 414 °C could be ascribed to the reduction of Bi_2O_3. Compared with the bulk Bi_2O_3, the highly dispersed Bi_2O_3 on the support could be reduced easily by H_2. The reduction peak of Co^{2+} also shifted to lower temperature after the deposition of Bi_2O_3, which might be induced by the interaction between the Bi_2O_3 and Co_3O_4. At the same time, a new sharp reduction peak β_4 was detected at about 615 °C, which also attributed to the reduction of Co^{2+}.

XRD results indicated that the doped Bi_2O_3 could enter the lattice of Co_3O_4, and produce the structure defects. The oxygen diffusion in bulk of Co_3O_4 was accelerated significantly due to the structure defects and the interaction between Bi_2O_3 and Co_3O_4, which induced the reduction of Co^{2+} in a narrow temperature range. It revealed the deposition of Bi_2O_3 could promote the reduction of Co_3O_4 and improve the oxygen mobility in the bulk Co_3O_4.

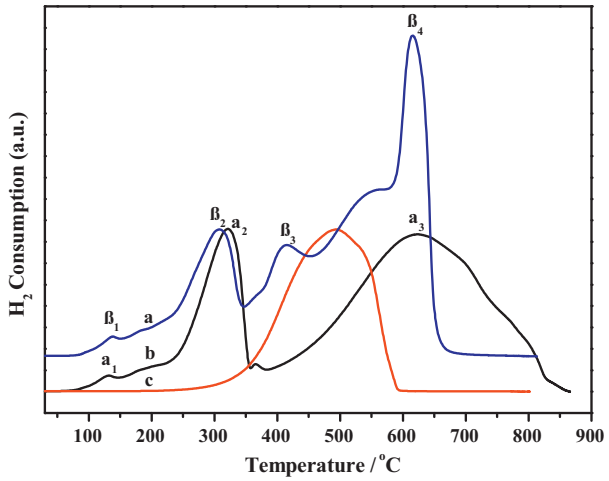

Fig. 3. H_2-TPR profiles of 20 wt.% Bi_2O_3–Co_3O_4 (a), Co_3O_4 (b) and Bi_2O_3 (c).

3.4. Raman spectra

Fig. 4 shows the Raman spectra of 20 wt.% Bi_2O_3–Co_3O_4 and pure Co_3O_4. For the pure Co_3O_4, there are five Raman-activated modes. The Raman peaks at 191, 481, 524, 617 and 688 cm^{-1} were corresponded to the $F_{2g}^{(3)}$, E_g, $F_{2g}^{(2)}$, $F_{2g}^{(1)}$ and O_h^7 symmetry of Co_3O_4 [28–30], respectively. 20 wt.% Bi_2O_3–Co_3O_4 gave the similar Raman spectra with Co_3O_4, while the characteristic peaks of Bi_2O_3 could not be detected [31,32]. Compared with Co_3O_4, the peak at 617 cm^{-1} disappeared, and all of the rest Raman peaks on 20 wt.% Bi_2O_3–Co_3O_4 shifted to the lower frequencies and broadened, which associated with the lattice distortion or residual stress of the spinel structure[33]. The XRD results showed that part of Bi_2O_3 entered the lattice of Co_3O_4 over 20 wt.% Bi_2O_3–Co_3O_4, the interaction between Co_3O_4 and Bi_2O_3 aroused the lattice distortion and lattice defect. The highly defective structure formed on 20 wt.% Bi_2O_3–Co_3O_4 could accelerate the adsorption and activation of O_2, which was suggested to be related to the better catalytic performance.

3.5. XPS characterization

Fig. 5 shows the Co 2p XPS spectra of Co_3O_4 and 20 wt.% Bi_2O_3–Co_3O_4. It is very difficult to detect Co^{2+} from Co^{3+} by Co 2p spectra because of the tiny difference in their binding energy (BE) values. The spin–orbit splitting of the Co 2p peaks (ΔE) was reported to be well correlated with the oxidation state of cobalt [9], the value of ΔE is 16.0 eV for CoO, 15.0 eV for Co_2O_3 [34], and

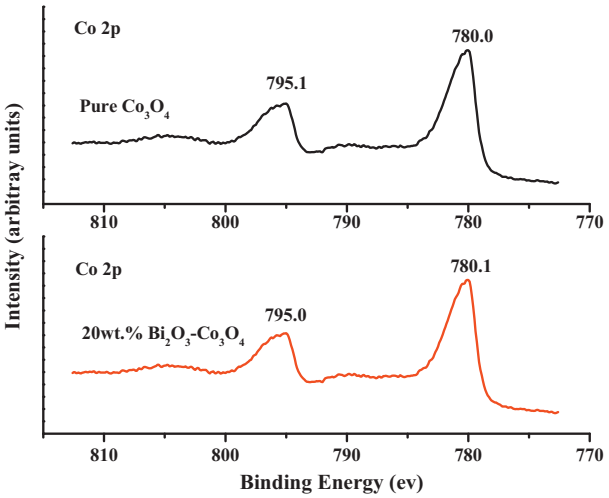

Fig. 5. XPS spectra of Co 2p on pure Co_3O_4 (a) and 20 wt.% Bi_2O_3–Co_3O_4 (b).

15.2 eV for the mixed-valence Co_3O_4 [35,36]. In our experiments, the ΔE value of Co 2p was 15.1 eV for the pure Co_3O_4, and 14.9 eV for 20 wt.% Bi_2O_3–Co_3O_4, which indicated the surface richness of Co^{3+} ions after the doping of Bi_2O_3. The Co^{3+} ions were regarded to be the active site for CO oxidation [10,13,37,38].

At the same time, Co 2p spectrum of 20 wt.% Bi_2O_3–Co_3O_4 shifted to lower binding energy. It indicated the decrease of electron binding ability of Co^{3+}, which further illustrated the enhancement of electron donor ability of Co^{3+} after the deposition of Bi_2O_3. Giamello [39] reported oxides with good qualities of electron conductivity were beneficial for oxygen activation on the vacancies. Hence, the increase of electron donor ability of Co^{3+} might also accelerate the activation of O_2 and produce more activated oxygen species, which improved the activity and stability of 20 wt.% Bi_2O_3–Co_3O_4 for CO oxidation greatly.

3.6. EPR spectra

The EPR spectra of pure Co_3O_4 and 20 wt.% Bi_2O_3–Co_3O_4 are showed in Fig. 6. In these catalysts, only Co^{2+} could be detected by EPR due to the unpaired electron of Co^{2+}[40]. The stronger peak intensity and larger peak area of Co^{2+} demonstrate that there are more Co^{2+} ions in 20 wt.% Bi_2O_3–Co_3O_4 than that in pure Co_3O_4,

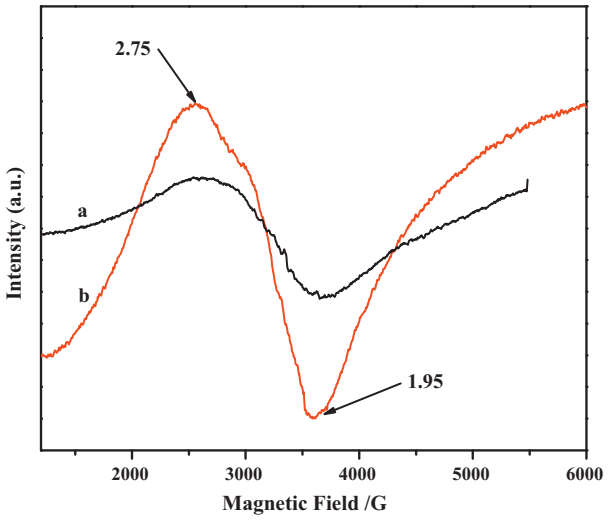

Fig. 6. EPR spectra obtained at room temperature, (a) pure Co_3O_4 and (b) 20 wt.% Bi_2O_3–Co_3O_4.

which implies more oxygen vacancies produced after the deposition of Bi_2O_3. However, the XPS results showed more Co^{3+} ions existing on the surface of 20 wt.% Bi_2O_3–Co_3O_4, which seemed to be contradict with the EPR results. It was reasonable to suggest that the doped Bi_2O_3 increased the Co^{3+} concentration on the surface, meanwhile, promoted the formation of Co^{2+} in the bulk phase. The richness of surface Co^{3+} could promote the adsorption and activation of CO, and the increase of Co^{2+} benefited the formation of oxygen vacancy.

The active surface oxygen species always exhibit great influence on the catalytic activity for low-temperature CO oxidation [41,42]. The oxygen vacancy can adsorb oxygen from the gas phase and weaken its bond to form the activated oxygen species [20,43]. The existence of a larger amount of oxygen vacancies could produce more activated oxygen species, which could accelerate the oxygen exchange and surface diffusion, and promote the catalytic ability of oxides for CO oxidation [43,44].

Many investigations have shown that the formation and accumulation of carbonate species on the surface can arouse the deactivation on the Co_3O_4 [10,45]. And when increasing the O_2 concentration, the deactivation rate could decrease and the activity could be improved [12]. The TPR, Raman and EPR results showed that more oxygen vacancies were produced on the Co_3O_4 after the doping of Bi_2O_3. The vacancy could accelerate the oxygen exchange and surface diffusion, which was suggested to be unavailable for the formation of carbonate species and slowdown the accumulation of carbonate species. Also, Bi_2O_3 behaved stronger Lewis acidity compared with Co_3O_4 [46,47], which could reduce the adsorption of CO_2 on the surface and decline the accumulation of carbonate species. It might be one of the reasons for 20 wt.% Bi_2O_3–Co_3O_4 owning the high activity and stability.

4. Conclusion

The Co_3O_4 and 20 wt.% Bi_2O_3–Co_3O_4 samples were prepared by precipitation and co-precipitation method. 20 wt.% Bi_2O_3–Co_3O_4 shows much better catalytic activity for CO oxidation than that of pure Co_3O_4. Under dry feed gas condition, after deposition of Bi_2O_3, the LTCC decreased from −40 °C on Co_3O_4 to −89 °C over 20 wt.% Bi_2O_3–Co_3O_4 catalyst. The complete CO conversion was maintained at −40 °C for 80 min over pure Co_3O_4, while 20 wt.% Bi_2O_3–Co_3O_4 can completely oxidize CO at −75 °C for 600 min. The doped Bi_2O_3 can enter the lattice of Co_3O_4 and induce the lattice distortion and structure defects. The reduction of Co_3O_4 was promoted by the structure defects and the interaction between Bi_2O_3 and Co_3O_4, especially for the reduction Co^{2+} in the bulk phase, which indicated the oxygen diffusion was accelerated remarkably.

XPS results showed the richness of Co^{3+} on the surface of 20 wt.% Bi_2O_3–Co_3O_4, which could promote the adsorption and activation of CO. The EPR results confirmed the increase of Co^{2+} in 20 wt.% Bi_2O_3–Co_3O_4, which could produce structure defects and lead to the formation of more oxygen vacancies. The oxygen vacancy accelerated the adsorption and activation of oxygen, and improved the diffusion of activate oxygen. It implied that the oxygen vacancy played the critical role in promoting the catalytic performance of 20 wt.% Bi_2O_3–Co_3O_4.

Acknowledgements

This project was supported financially by the National Basic Research Program of China (2010CB732300), the National Key Technologies R & D Program of China (2007BAJ03B01), and the National Natural Science Foundation of China (20601008).

References

[1] S.A.C. Carabineiro, B.F. Machado, R.R. Bacsab, P. Serpb, G. Dražić, J.L. Faria, J.L. Figueiredo, J. Catal. 273 (2010) 191.
[2] S.Y. Li, G. Liu, H.L. Lian, M.J. Jia, G.M. Zhao, D.Z. Jiang, W.X. Zhang, Catal. Commun. 9 (2008) 1045.
[3] M. Haruta, T. Kobayashi, N. Yamada, Chem. Lett. 16 (1987) 405.
[4] M.S. Chen, D.W. Goodman, Science 306 (2004) 252.
[5] B.T. Qiao, L.Q. Liu, J. Zhang, Y.Q. Deng, J. Catal 261 (2009) 241.
[6] J. Luo, M. Meng, X. Li, X. Li, Y. Zha, T. Hu, Y. Xie, J. Zhang, J. Catal. 254 (2008) 310.
[7] H. Tüysüz, M. Comotti, F. Schüth, Chem. Commun. 34 (2008) 4022.
[8] L.H. Hu, K.Q. Sun, Q. Peng, B.Q. Xu, Y.D. Li, Nano Res. 3 (2010) 363.
[9] J. Jansson, A.E.C. Palmqvist, E. Fridell, M. Skoglundh, L. Österlund, P. Thormählen, V. Langer, J. Catal. 211 (2002) 387.
[10] X.W. Xie, Y. Li, Z.Q. Liu, M. Haruta, W.J. Shen, Nature 458 (2009) 746.
[11] K. Omata, T. Takada, S. Kasahara, M. Yamada, Appl. Catal. A: Gen. 146 (1996) 255.
[12] H.C. Yao, M. Shelef, J. Phys. Chem. 78 (1974) 2490.
[13] P. Broqvist, I. Panas, H. Persson, J. Catal. 210 (2002) 198.
[14] C.J. Jia, Y. Liu, H. Bongard, F. Schüth, J. Am. Chem. Soc. 132 (2010) 1520.
[15] L.Q. Liu, F. Zhou, L.G. Wang, X.J. Qi, F. Shi, Y.Q. Deng, J. Catal. 274 (2010) 1.
[16] J. Jansson, J. Catal. 194 (2000) 55.
[17] P. Thormählen, M. Skoglundh, E. Fridell, B. Andersson, J. Catal. 188 (1999) 300.
[18] Y.B. Yu, T. Takei, H. Ohashi, H. He, X.L. Zhang, M. Haruta, J. Catal. 267 (2009) 121.
[19] D. Widmann, R. Leppelt, R.J. Behm, J. Catal. 251 (2007) 437.
[20] V. Shapovalov, H. Metiu, J. Catal. 245 (2007) 205.
[21] S. Chretien, H. Metiu, Catal. Lett. 107 (2006) 143.
[22] A. Trovarelli (Ed.), Catalysis by Ceria and Related Materials, Imperial College Press, London, 2002.
[23] L. Xue, C.B. Zhang, H. He, Y. Teraoka, Appl. Catal. B 75 (2007) 167.
[24] P.G. Harrison, I.K. Ball, W. Daniell, P. Lukinskas, M. Céspedes, E.E. Miró, M.A. Ulla, Chem. Eng. J. 95 (2003) 47.
[25] N. Bahlawane, E.F. Rivera, K.K. Höinghaus, A. Brechling, U. Kleineberg, Appl. Catal. B 53 (2004) 245.
[26] H.Y. Lin, Y.W. Chen, Mater. Chem. Phys. 85 (2004) 171.
[27] B. Mazumder, J.C. Védrine, Appl. Catal. A: Gen. 245 (2003) 87.
[28] L. He, Z. Li, Z. Zhang, Nanotechnology 19 (2008) 155606.
[29] V.G. Hadjievl, M.N. Ilievl, I.V. Vergilov, J. Phys. C: Solid State Phys. 21 (1988) l99.
[30] Q. Liu, L.C. Wang, M. Chen, Y. Cao, H.Y. He, K.N. Fan, J. Catal. 263 (2009) 104.
[31] S.N. Narang, N.D. Patel, V.B. Kartha, J. Mol. Struct. 327 (1994) 221.
[32] M. Prekajski, A. Kremenović, B. Babić, M. Rosić, B. Matović, A.R. Mihajlović, M. Radović, Mater. Lett. 64 (2010) 2247.
[33] I. Lopes, N.E. Hassan, H. Guerba, G. Wallez, A. Davidson, Chem. Mater. 18 (2006) 5826.
[34] Z.M. Liu, J.M. Hao, L.X. Fu, T.L. Zhu, Appl. Catal. B 44 (2003) 355.
[35] D.V. Cesar, C.A. Peréz, M. Schmal, V.M.M. Salim, Appl. Surf. Sci. 157 (2000) 159.
[36] H. Wang, H.Q. Zhu, Z.F. Qin, F.X. Liang, G.F. Wang, J.G. Wang, J. Catal. 264 (2009) 154.
[37] M. Kang, M.W. Song, C.H. Lee, Appl. Catal. A 251 (2003) 143.
[38] Q. Guo, Y. Liu, Appl. Catal. B 82 (2008) 19.
[39] E. Giamello, Catal. Today 41 (1998) 239.
[40] P.B. Jiang, T.X. Cheng, Y. Liu, X.H. Cui, Y.L. Bi, K.J. Zhen, React. Kinet. Catal. Lett. 82 (2004) 49.
[41] C. Ma, Z. Mu, J. Li, Y. Jin, J. Cheng, G. Lu, Z. Hao, S. Qiao, J. Am. Chem. Soc. 132 (2010) 2608.
[42] S. Chavadej, K. Saktrakool, P. Rangsunvigit, L.L. Lobban, T. Sreethawong, Chem. Eng. J. 132 (2007) 345.
[43] Z.P. Hao, D.Y. Cheng, Y. Guo, Y.H. Liang, Appl. Catal. B 33 (2001) 217.
[44] W. Liu, M.F. Stephanopoulos, Chem. Eng. J. 64 (1996) 283.
[45] F. Grillo, M.M. Natile, A. Glisenti, Appl. Catal. B 48 (2004) 267.
[46] M.A. Centeno, M.J. Capitan, P. Bosch, P. Malet, J.J. Benitez, L. Carrizosaa, J.A. Odriozola, J. Mater. Chem. 5 (1995) 175.
[47] G. Busca, Phys. Chem. Chem. Phys. 1 (1999) 723.